Simultaneously Enhanced Stability and Selectivity for Propene Epoxidation with H_2 and O_2 on Au Catalysts Supported on Nano-Crystalline Mesoporous TS-1

Xiang Feng,† Nan Sheng, † Yibin Liu, † Xiaobo Chen, † De Chen, § Chaohe Yang† and Xinggui Zhou‡**

† State Key Laboratory of Heavy Oil Processing, School of Chemical Engineering, China University of Petroleum, Qingdao 266580, China.

‡ State Key Laboratory of Chemical Engineering, East China University of Science and Technology, Shanghai 200237, China.

§ Department of Chemical Engineering, Norwegian University of Science and Technology, Trondheim 7491, Norway.

ABSTRACT: It is a challenging task to design efficient Au/Ti-containing catalysts for propene epoxidation with H_2 and O_2 that simultaneously achieve high catalytic stability and selectivity to propylene oxide (PO). This contribution first describes the synthesis of a nano-crystalline mesoporous titanium silicalite-1 (MTS-1) by dry-gel conversion that employs cheap triblock copolymers as template. Compared with TS-1, MTS-1 has shortened reactant/product diffusion length as a result of smaller crystal size (<100 nm) and presence of mesopores (ca. 3 nm). Surprisingly, this designed catalyst shows simultaneously improved PO selectivity over 95% as well as stability over 40 h, much better than traditional Au/TS-1 catalyst. Moreover, the intrinsic reason for the enhanced performance is elucidated. The better mass transfer ability together with higher hydrophobicity of Au/MTS-1 result in lower coke weight and absence of refractory aromatic coke. In this way, the side reactions and deactivation caused by blocking of micropore are inhibited.

KEYWORDS: Propene epoxidation; Stability; Selectivity; Mass transfer; Au/TS-1.

1 Introduction

Propylene oxide (PO), the third largest propene derivative, is recognized as a high value-added chemical intermediate for the manufacture of polyurethane and polyether resins.[1] In comparison to conventional methods to produce PO, the direct propene epoxidation with H_2 and O_2 has attracted immense research interest because it is environmentally benign, simple and sustainable.[2] Since the discovery that Au/TiO_2 could achieve high selectivity towards PO production in 1998[3], extensive studies have focused on designing efficient Au catalysts.[4] Of the reported Au/Ti-based catalysts (e.g., Au/TS-1, Au/Ti-TUD, Au/three-dimensional mesoporous titanosilicate, Au/Ti-HMS and Au/Ti-SiO_2), the hydrophobic TS-1 supported Au catalyst exhibits the superior activity and stability.[2, 5-13] Unfortunately, even Au/TS-1 catalysts still suffer from severe deactivation with a decay of ca. 30% activity in only 20 h.[2] Several strategies have been proposed to improve the stability of Au/TS-1 catalysts by various preparation methods,[14-17] such as sol-immobilization (SI) [15, 16] and solid-grinding (SG).[17, 18] Although Au/TS-1-SI and Au/TS-1-SG catalysts exhibit better stability, the PO selectivity decreased from 92% to ca. 70-87%. Therefore, it is of prime scientific and industrial importance to design a highly efficient catalyst with simultaneously improved PO selectivity and stability.

We have reported that the deactivation of Au/TS-1 is mainly because the diffusion limitation of molecules in the narrow micropore channels of TS-1 (~0.55 nm) results in a poor access of reactants to the Au-Ti active sites, and more severely, the blocking of the diffusion path.[19] The micropore blocking by carbonaceous deposits, which are formed by the initial PO adsorption on the catalyst surface and subsequent oligomerization, rearrangement, cracking, coupling and so on,[10, 18, 20] makes Au clusters inside micropores inaccessible to reactants.[14] Therefore, from the

analysis of the deactivation mechanism, making use of the concept of mass transfer enhancement[21] by decreasing the diffusion path length[22] of products inside zeolite seems to be a promising scenario for this problem. This could be achieved by developing a hierarchical zeolite and reducing the crystal size of the zeolite.[23-25] The hierarchical TS-1 in the form of nano-sized crystals would display decreased diffusion path length and increased external surface area. On the one hand, the improved mass transfer ability could improve the stability by providing easier access to active sites and enhancing resistance to coke formation. On the other hand, the enhanced mass transfer ability could improve the PO selectivity by facilitating PO desorption and subsequently suppressing side reactions on catalyst surface (e.g., ring-opening of PO). However, little attention has been paid on synthesizing novel mesoporous and small-sized TS-1 supported Au catalysts for propene epoxidation with H_2 and O_2. It is thus highly desired to design novel Au/Ti-containing catalyst for this reaction. Moreover, understanding the effects of structural properties of support on catalytic selectivity and stability will undoubtedly be beneficial to improving the performance of the Au/Ti-containing catalyst for PO synthesis.

Herein, we demonstrate for the first time that it is possible for an Au/Ti-containing catalyst to achieve simultaneously improved PO selectivity and catalytic stability. We propose a facile route for synthesizing a novel nano-crystalline mesoporous TS-1 (MTS-1) by the dry-gel conversion method with the aid of cheap triblock copolymer. Compared with the hydrothermal synthesis, this dry-gel route has the advantages of high yield and significant reduction of pollutants, which show good potential for industrial application. Moreover, the relationship between the physico-chemical structure of Au/TS-1 catalyst and catalytic performance (i.e., PO selectivity and catalytic stability) is further elucidated. The better mass transfer ability together with higher hydrophobicity result in lower coke formation and absence of refractory aromatic coke, inhibiting the side reactions and

deactivation caused by blocking of micropores and active sites. The results will be of great importance to the design and synthesis of highly efficient supported zeolite catalysts that suffer from poor stability and selectivity.

2 Experimental

2.1 Catalyst preparation

The MTS-1 support was synthesized according to the following procedure. First, 173 mmol tetraethylorthosilicate (TEOS, 95 wt%) were added to 22.6 g tetrapropylammonium hydroxide (TPAOH, 25 wt%). Afterwards, a required amount of titanium (IV) tetrabutoxide (TBOT, 99 wt%) dissolved in 20 mL isopropanol (IPA, 99.5 wt%) was added drop-wise. The above sol was added into triblock copolymers P123 solution, aged at 333 K overnight and subsequently dried at 363 K for at least 12 h until the mass of the solid gel became unchanged. The gel was crystallized by steam-assisted crystallization method at 443 K for at least 18 h. The product was washed and dried overnight at room temperature, and then calcined at 823 K for 5.5 h to remove the template. The as-obtained product was labelled as MTS-1. The TS-1 with Si/Ti ratio of 100 was synthesized using hydrothermal method developed by Khomane et al.[15]

The TS-1 and MTS-1 supports were used to deposit Au nanoparticles by deposition-precipitation method.[14] In a typical process, 0.5 g TS-1 and MTS-1 supports were added into the mixture of 10 mL $HAuCl_4 \cdot 3H_2O$ and 40 mL deionized water. The slurry was neutralized to pH of 7.3 by 1 M aqueous solution of sodium hydroxide, and then aged at room temperature for different hours. Finally, these catalysts were centrifuged for 30 min and dried at room temperature overnight under vacuum.

2.2 Characterization

The X-ray diffraction patterns (XRD) of MTS-1 and TS-1 supports were collected on a Rigaku D/Max2550VB/PC X-ray diffractometer using Cu Kα radiation. The N_2 adsorption-desorption isotherms were measured on a Micromeritics ASAP 2020 instrument. The ultraviolet-visible spectroscopy (UV-vis) was determined on a Perkin Elmer Lambda 35 spectrophotometer. The weight of carbonaceous deposits was analyzed by thermogravimetric analysis (TGA, Perkin Elmer TGA Pyris 1). The TGA analysis was performed by heating dried sample from room temperature to 800^{o}C in a flow of N_2/O_2=8:1 at a ramping rate 5^{o}C/min. The high resolution transmission electron microscopy (HRTEM) images were obtained on a JEOL JSM-2100 microscope, while the scanning electron microscopy (SEM) images were taken on a NOVA Nano SEM450 microscope. The fourier transform infrared spectroscopy (FT-IR) spectra of the catalysts were obtained on a Nicolet 6700 spectrometer. Au loadings were determined by the atomic absorption spectroscopy (AAS) on a ZEEnit 600 spectrometer. High-angle annular dark-field scanning transmission electron microscopy (HAADF-STEM) was obtained on a Tecnai G2 F20 S-Twin equipped with a digitally processed STEM imaging system.

2.3 Catalytic testing

The gas-phase propene epoxidation with H_2 and O_2 was carried out in a quartz tubular reactor (i.d. 8 mm) using a feed containing C_3H_6, H_2, O_2 and N_2 with the flow rate of 3.5/3.5/3.5/24.5 mL·min^{-1}. The Au/TS-1 and Au/MTS-1 catalysts (0.15 g) were tested under atmospheric pressure. The products were analysed by two on-line GCs (Agilent 6890). Hydrocarbons, H_2, O_2, N_2, CO_x and H_2O were analyzed by GC equipped with TCD (5A and Porapak Q column). Oxygenates (e.g., propene, propane, acetaldehyde, PO, acetone and propanal) were analyzed with the other GC

equipped with FID (Porapak T column). Blank tests indicated that no PO was generated in the blank reactor.

Propene conversion = mol of (C_3-oxygenates + 2/3ethanal + CO_2/3)/mol of propene in the feed.

PO selectivity = mol of PO/mol of (C_3-oxygenates + 2/3ethanal + CO_2/3).

H_2 efficiency = mole of PO/mol of H_2 converted.

3 Results and discussion

3.1 Simultaneously enhanced performance of Au/MTS-1 catalyst

The physico-chemical properties of MTS-1 and TS-1 are first examined. The XRD patterns of the two samples (Figure 1a) show similar diffraction peaks located at 2θ=7.9º, 8.8º, 23.1º, 23.9º and 24.3º, which confirm the MFI topological structure of TS-1 and MTS-1. Both TS-1 and MTS-1 have single peaks at 2θ=24.3º, demonstrating the structure has a orthorhombic unit cell.[26] Compared with TS-1, the MTS-1 sample has the broadening of XRD diffraction peaks, which indicates the decrease of the crystal size.[27] TEM and SEM are preferred to calculate the TS-1 particle size since Scherrer's equation by XRD can only be applied for average sizes up to about 100-200 nm. Figure 1b shows the N_2 adsorption-desorption isotherms of the TS-1 and MTS-1 samples with the pore size distribution of MTS-1 in the inset. TS-1 exhibits a typical type I isotherm according to IUPAC's classification, demonstrating the microporous characteristic.[28] The neglectable uptake in the isotherm of TS-1 at P/P_0>0.1 reveals the absence of mesoporosity. For MTS-1 support, the sharp uptake at P/P_0<0.02 indicates the presence of micropores. In addition, a type IV isotherm is observed, suggesting the presence of mesopores. The hysteresis loop at p/p_0 range of 0.7-0.9 is observed, which is due to multilayer adsorption of nitrogen molecules inside

mesopores.[29] From the pore size distribution in Figure 1b, it is concluded that the MTS-1 sample has a mesopore size of 2.8 nm and a wide distribution larger than 10 nm, which are assigned to intracrystalline and intercrystalline mesopores (i.e., the aggregation of small crystallites), respectively. In contrast, no mesopores exist on TS-1 sample. The mesoporosity of MTS-1 support is also confirmed by the much larger mesopore volume (Table S1).

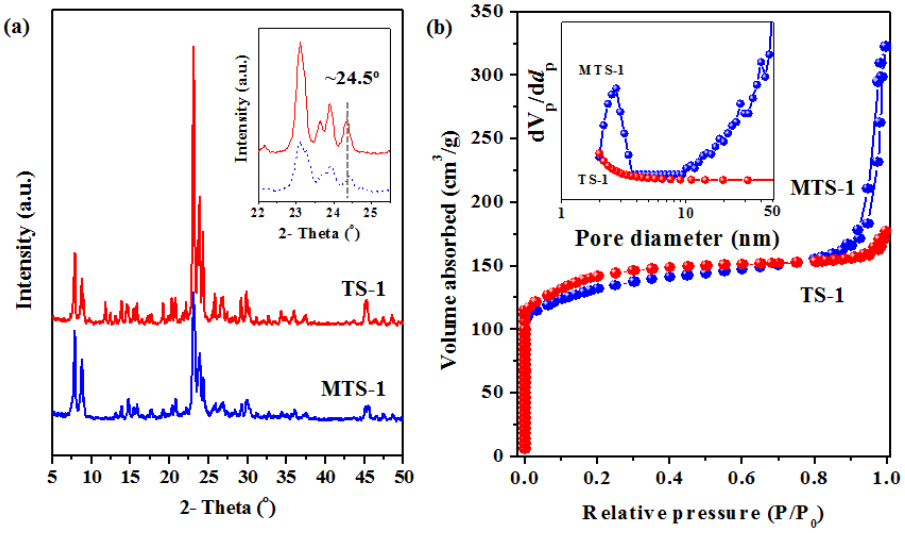

Figure 1. XRD patterns (a) and N_2 adsorption-desorption iso-therms (b) of MTS-1 and TS-1 supports. The inset in Figure 1b shows the pore size distribution of MTS-1 and TS-1.

Figure 2a shows the FT-IR spectra of the TS-1 and MTS-1 samples. The adsorption band at 550 cm^{-1} is assigned to the vibration of the double five-membered ring unit and certificates the presence of MFI structure, which is in accordance with the XRD results. The bands at 800 and 1100 cm^{-1} are due to the symmetrical and antisymmetrical stretching vibration of [SiO_4] units, respectively. In addition, the band at 1230 cm^{-1} is attributed to the asymmetrical stretching vibration of MFI framework structure. The band at 960 cm^{-1} is often considered as a proof of Ti substitution into the framework in the form of Ti-O-Si.[30, 31] The Ti environment in the TS-1 framework is essential

for the catalytic performance. It can be determined by UV-vis characterization (Figure 2b). There is consent that only isolated Ti (IV) species are responsible for selective propene epoxidation with H_2 and O_2.[32] It is clear that one adsorption peak at ca. 220 nm exist for the two samples, confirming the presence of isolated Ti (IV) species in the MFI framework. In addition, no adsorption peaks attributed to anatase TiO_2 species show up at 330 nm[5].

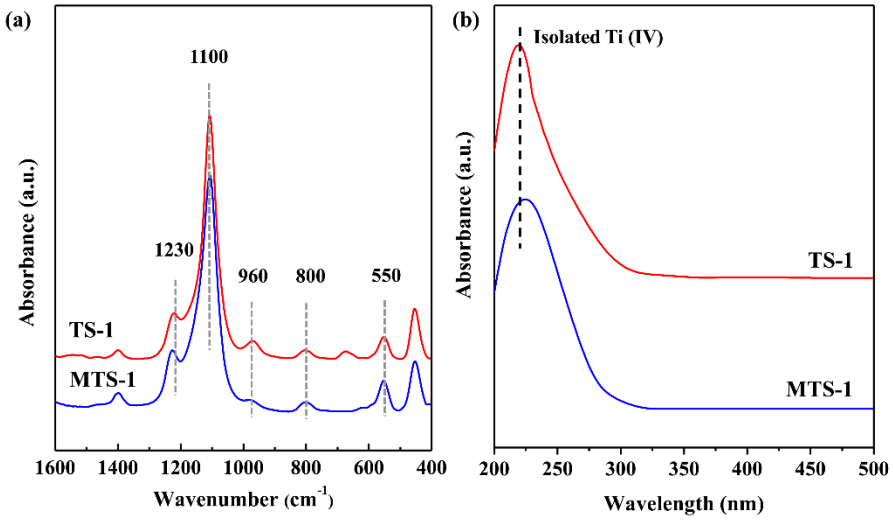

Figure 2. FT-IR spectra (a) and UV-vis spectra (b) of MTS-1 and TS-1 supports.

The shapes of the TS-1 and MTS-1 supports are shown in Figure 3(a,b). Both are regular and coffin-like. Compared with TS-1, which has a larger particle size of ca. 500 nm, the MTS-1 sample exhibits a significantly reduced particle size of smaller than 100 nm. This could be ascribed to the different crystallization conditions of the hydrothermal and dry-gel conversion methods. In contrast to the hydrothermal method, a large number of nuclei may be formed in the aging stage of the dry-gel conversion process as a result of the highly concentrated precursor in the dry-gel.[33] These nuclei have limited nutrition and are not likely to grow into large crystals by Ostwald ripening because of the nearly dry environment. Figure 3(c,d) show the typical TEM images of the two samples. The surface of the TS-1 support is smooth, nevertheless, uniform mesopores are

present on the MTS-1 sample. The mean mesopore size is ca. 3 nm, which agrees well with the pore size estimated from the BJH pore size distribution of 2.8 nm (Figure 1b). Furthermore, the lattice fringes can be clearly seen in the framework of the MTS-1 sample (Figure S1), revealing that the whole framework could be assigned as a single crystal with penetrating mesoporous network inside.

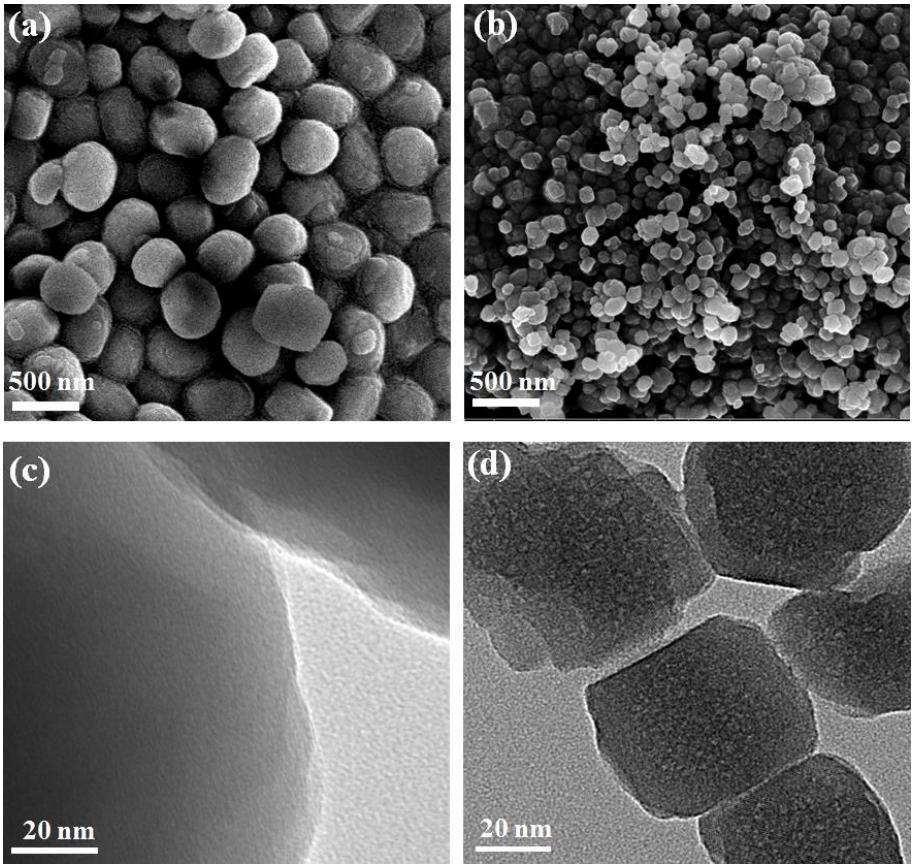

Figure 3. SEM and TEM images of TS-1 (a, c) and MTS-1 supports (b, d).

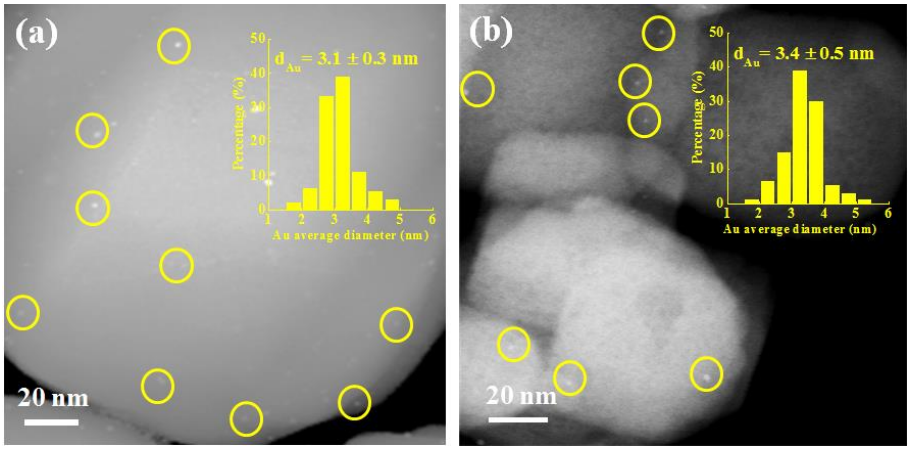

Figure 4. HAADF-STEM images of Au/TS-1 (a) and Au/MTS-1 catalysts (b). The insets show the Au size distributions of the catalysts, and the scale bars represent 20 nm.

Figure 4 shows the HAADF-STEM images of the Au/TS-1 and Au/MTS-1 catalysts. In order to increase accuracy, more than 150 nanoparticles were measured to determine Au particle size distribution. For the observable Au nanoparticles, the average Au nanoparticle size of the Au/MTS-1 catalyst (3.4 nm) is slightly larger than that of the Au/TS-1 catalyst (3.1 nm). Besides the average particle size, it should be noted that the Au size distribution is also essential to evaluate the Au sizes. It can be seen from the Au size distributions in the insets that the sizes of most Au nanoparticles range from 2.5 to 3.5 nm for Au/TS-1 catalyst. In contrast, those for Au/MTS-1 catalyst range from 3.0 to 4.0 nm.

The catalytic performance of the Au/MTS-1 and the conventional Au/TS-1 catalysts for propene epoxidation are compared in Figure 5. To make a fair comparison, the Au loadings of the two catalysts are similar (ca. 0.1 wt%). The Au/TS-1 catalyst shows higher initial PO formation rate (170 $g_{PO}h^{-1}kg_{Cat}^{-1}$) because part of the tiny Au clusters incorporated in the microporous channels of TS-1 are highly active towards PO production.[34-36] However, the PO formation rate sharply decreased from 170 to 128$g_{PO}h^{-1}kg_{Cat}^{-1}$ because the Au clusters inside the microporous channels

are no longer accessible to reactants due to micropore blocking deactivation by carbonaceous deposits.[12] In contrast, the Au/MTS-1 catalysts show greatly improved stability for over 40 h. Increasing Au loading from 0.07 to 0.13wt%, the PO formation rate increased from 75 to 142$g_{PO}h^{-1}kg_{Cat}^{-1}$.

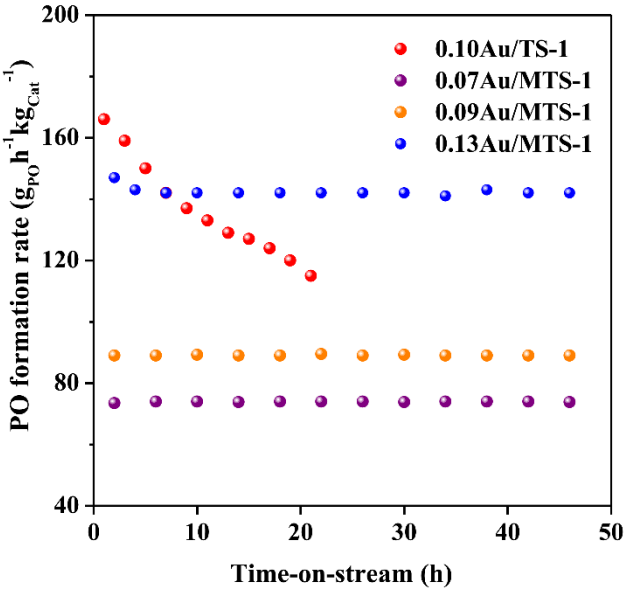

Figure 5. PO formation rate of Au/TS-1 and Au/MTS-1 catalysts at different time-on-steam.

Figure 6 shows the selectivities of the catalysts. For traditional Au/TS-1 catalyst, the PO selectivity is ca. 89%. However, all of Au/MTS-1 catalysts exhibit PO selectivity higher than 95%, much better than that of the traditional Au/TS-1 catalyst. This is possibly because better mass transfer ability facilitates the desorption of PO, and thus inhibits the ring-opening reaction of PO to side products (e.g., CO_2, ethanal, propanal).[37] Figure 6b shows the detailed product selectivities and H_2 efficiencies of the Au/TS-1 and Au/MTS-1 catalysts. The main side products of Au/TS-1 and Au/MTS-1 catalysts were all propanal and carbon dioxide. In addition, the H_2 efficiency is also higher on the Au/MTS-1 catalyst. It is noted that hydrogenation of H_2O_2 to H_2O and decomposition of H_2O_2 to H_2O_2 and O_2 are two routes to decrease H_2 efficiency.[38] However, the

decomposition of H_2O_2 may be more predominant at high temperature of 200°C.[5] Hence, the enhanced mass transfer ability facilitates the transmission of H_2O_2 from Au to nearby Ti^{4+} sites, thus inhibiting the decomposition of H_2O_2 to H_2O.

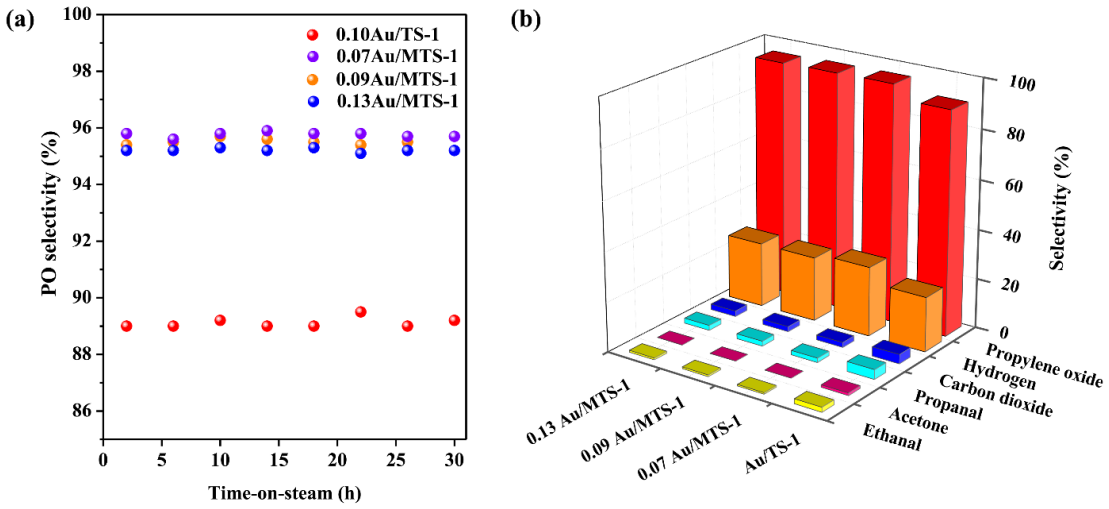

Figure 6. PO selectivities (a) and detailed products distributions and H_2 efficiencies (b) of 0.10wt% Au/TS-1 and Au/MTS-1 catalysts with Au loadings of 0.07, 0.09 and 0.13wt%.

3.2 Intrinsic reason for the unique performance of Au/MTS-1 catalyst

In order to elucidate the intrinsic reason for the unique performance of the Au/MTS-1 catalyst, the properties of the catalysts after reaction were further analyzed. The TGA results of the Au/TS-1 and Au/MTS-1 catalysts at 200 °C after 30 h are shown in Figure 7a. The total coke weight of the Au/MTS-1 catalyst (i.e., 2.8 wt%) was much lower than that of the Au/TS-1 catalyst (i.e., 4.9 wt%), suggesting that coke formation on the Au/MTS-1 catalyst is effectively alleviated. It is accepted that the coke formation is associated with the diffusion length of reactants/products in the micropores of the zeolite.[39] Shorter diffusion length usually results in less coke. Although coke still exists on the Au/MTS-1 catalyst, the presence of mesopores may make the micropore blocking deactivation difficult to take place. Figure 7b shows the DTG curves of the Au/TS-1 and Au/MTS-

1 catalysts. For Au/TS-1 catalyst, three DTG peaks center at 340, 460 and 650 ^{o}C, which originate from the oxidation of different kinds of carbonaceous deposits on the surface of the used catalyst. Usually, heavier carbonaceous deposits show up at higher temperature. The DTG peak at 650^{o}C, corresponding to refractory carbonaceous deposits, does not exist on the Au/MTS-1 catalyst. Therefore, the carbonaceous deposits on Au/TS-1 are much heavier than those on Au/MTS-1 catalyst.

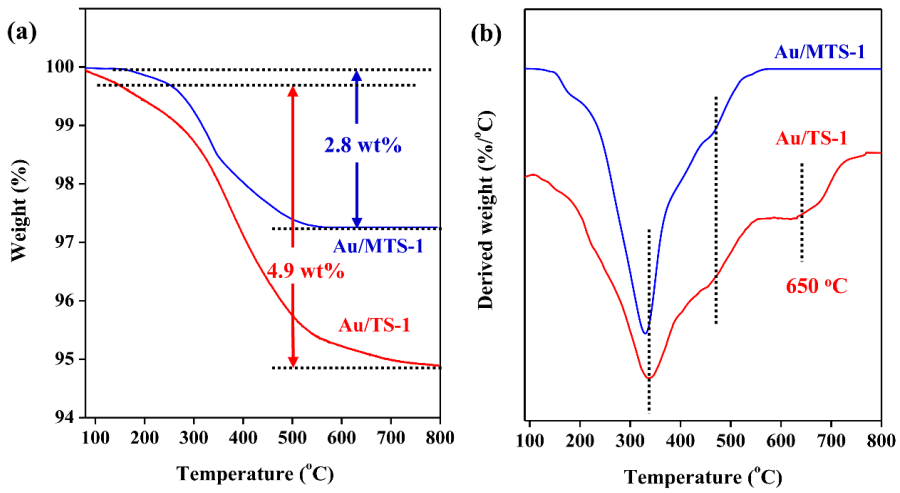

Figure 7. TGA (a) and DTG (b) curves of Au/TS-1 and Au/MTS-1 catalysts at 200^{o}C for 25 hours.

FT-IR was also employed to investigate the properties of these refractory carbonaceous deposits (Figure 8). For the Au/MTS-1 catalyst, two bands are observed at 1350-1470 and 1600-1650 cm^{-1}, which are attributed to branched alkanes and polyalkenes,[40] respectively. In contrast, a unique band at 1700-1750 cm^{-1}, which is ascribed to refractory aromatic species,[40] is observed for the traditional Au/TS-1 catalyst. Besides the reduced coke weight (Figure 7), the reduced diffusion length of reactants and products (i.e., better mass transfer ability) leads to the absence of refractory aromatic species in Au/MTS-1 catalysts.

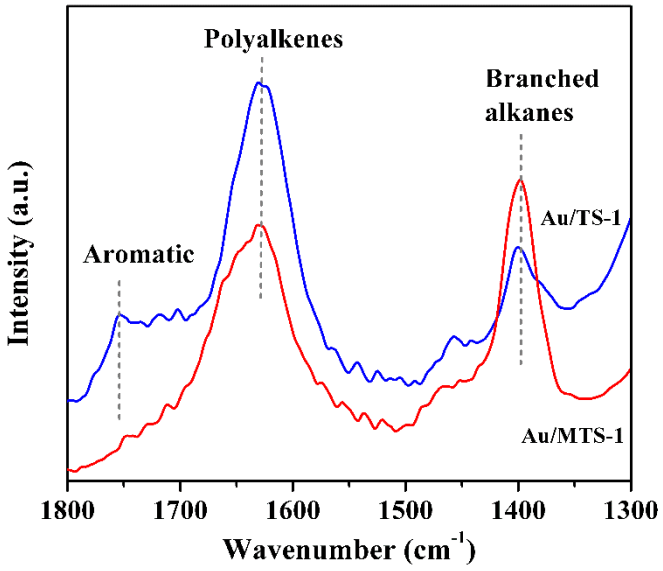

Figure 8. FT-IR spectra of Au/TS-1 and Au/MTS-1 catalysts at 200°C for 25 hours.

Besides the mass transfer ability, hydrophobicity is another key parameter affecting the properties of carbonaceous deposits.[8] Figure 9 shows the ^{29}Si MAS NMR spectra of the two samples. All spectra show the absence of $(SiO)_2Si(OH)_2(Q_2)$ resonances at approximately -80 to -90 ppm. This is strong corroborating evidence that there is no amorphization of the zeolite framework. Both samples exhibit strong signals at -113 and -104 ppm in the ^{29}Si spectra, which are associated with typical $Si(OSi)_4(Q_4)$ and $(SiO)_3SiOH(Q_3)$ species, respectively. The shoulder at -116 ppm is attributed to the orthorhombic symmetry of zeolite.[41] The signal at -104 ppm in the spectrum of TS-1 corresponding to the Si species functionalized by hydroxyl groups (Q_3)[22, 42, 43] is stronger than that of MTS-1. Upon deconvolution and integration of the spectra, the percentages of hydroxyl-attached Si (-104 ppm) are 5.8 and 3.3% for TS-1 and MTS-1, respectively, demonstrating that the MTS-1 has less hydroxyl groups than TS-1 support. The decrease of surface hydroxyl groups indicates an increase of hydrophobicity, which is beneficial for the desorption of PO and suppression of side reactions on catalyst surface. Besides better mass transfer ability, this

higher hydrophobicity also gives explanation on the less refractory carbonaceous deposits of Au/MTS-1 catalyst.

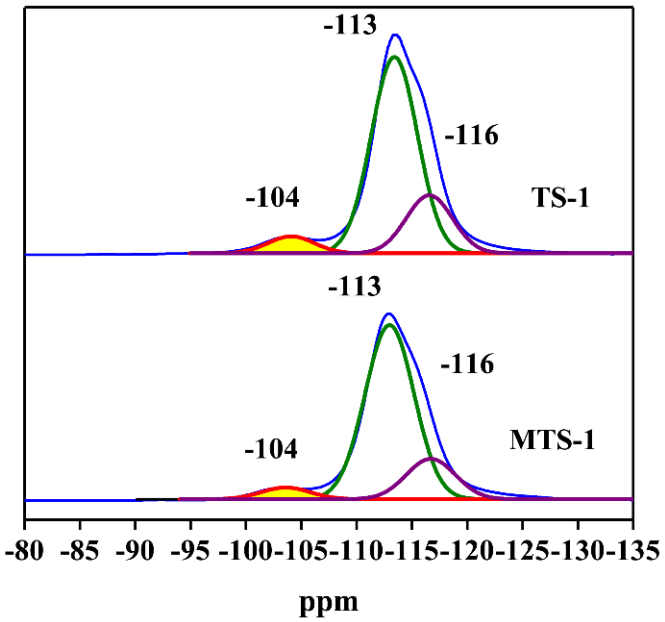

Figure 9. ^{29}Si MAS NMR spectra of TS-1 and MTS-1 supports.

Au/TS-1 is a bi-functional catalyst for propene epoxidation with H_2 and O_2, and the Au-Ti site is considered as the catalytic site. It is reported that Au sites are mainly responsible for formation of H_2O_2, and Ti sites are responsible for propene epoxidation to PO by Ti-OOH intermediate.[34] In a typical process, the absorbed PO could open its ring to form the branched alkanes,[10] which are further converted into polyalkenes and subsequent aromatic species. Compared with Au/TS-1, the Au/MTS-1 catalyst has shortened diffusion length (reduced TS-1 size and presence of mesopores[44,45]) and higher hydrophobicity, which hamper the evolution and formation of refractory carbonaceous deposits. Therefore, Au/MTS-1 catalyst shows more branched alkanes, less polyalkenes and absence of aromatic species. This should be one of the main reasons for the enhanced stability for Au/MTS-1 catalyst. Moreover, the existence of mesopores will also leave more room for carbonaceous deposits, making micropore blocking less possible. As a consequence,

the inevitable presence of coke on Au/MTS-1 catalysts could not easily block the microporous channels. With respect to PO selectivity, the higher hydrophobicity and enhanced mass transfer ability could facilitate PO desorption and subsequently suppresses side reactions on catalyst surface. This greatly improves the PO selectivity of Au/MTS-1 catalyst (Figure 10).

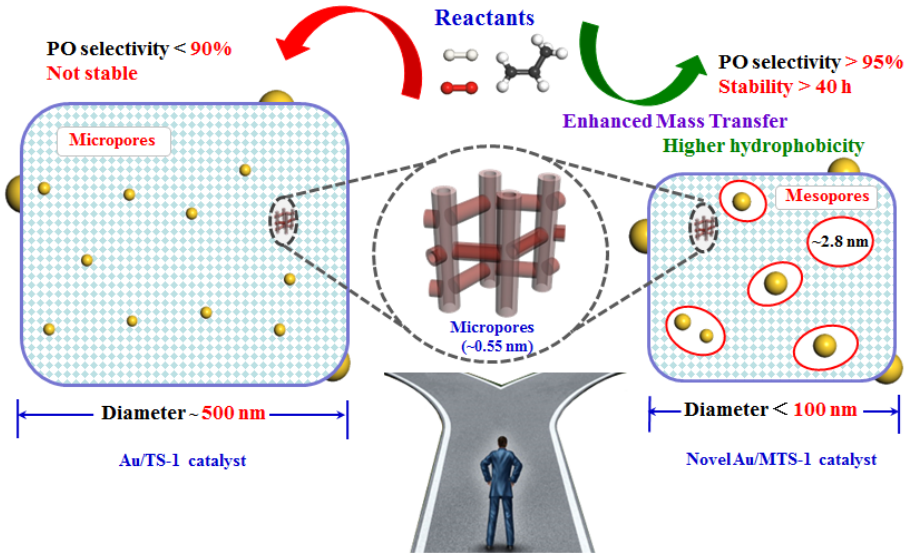

Figure 10. Possible reason for the enhanced catalytic performance of Au/MTS-1 catalysts.

Table 1 displays a comparison of the catalytic performance of Au/MTS-1 and Au/Ti-containing catalysts taken from literature. Compared with the reported Au catalysts[2,16,18,46-48] which have only high selectivity or stability (Table 1), the Au/MTS-1 catalyst has simultaneously improved PO selectivity as well as high stability at 473 K. It is possible that other hierarchical TS-1 support with good hydrophobicity may also be suitable for propene epoxidation with H_2 and O_2 due to better PO desorption and subsequent suppression of side reactions on the catalyst surface. Moreover, locating Au clusters on the openings of TS-1 may also be a possible scenario to achieve high catalytic performance for PO formation. This is an interesting topic, which will be carried out in our future study. This work is of significant importance for the design and synthesis of other efficient supported metal catalysts that suffer from severe deactivation and poor selectivity.

Table 1. The catalytic properties of Au/Ti-containing catalysts for propene epoxidation with H_2 and O_2.

Samples	Au loading (wt%)	PO selectivity (%)	Stability (h)	PO formation rate ($g_{PO}h^{-1}kg_{Cat}^{-1}$)	Reaction temperature (K)	Reference
Au/MTS-1[a]	0.13	95.2	40	142	473	This work
Au/Ti-MCM-36	0.84	94.5	Not stable[b]	8	433	46
Au/TS-1	0.10	90.0	Not stable[b]	150	473	2
Au/Ti-SiO_2	0.05	89.4	6	63	473	47
Au/TS-1-SG	0.10	85.0	16	119	473	18
Au/Ti-YNU-1	0.28	80.1	Not stable[b]	29	498	48
Au/TS-1-IL	1.0	65.0	48	75	573	16

[a] Reaction condition: 0.15g catalyst; feed gas, $C_3H_6/H_2/O_2/N_2$=3.5/3.5/3.5/22.5 cm^3min^{-1}, space velocity=14000 $mLg_{Cat}^{-1}h^{-1}$; feed pressure=1atm; reaction temperature=473 K;

[b] Not stable means the catalyst deactivates quickly when the reaction starts.

4 Conclusions

In summary, we have demonstrated that it is possible to simultaneously improve the catalytic selectivity and stability of Au/Ti-containing catalysts for the green and simple propene epoxidation with H_2 and O_2 by enhancing the mass transfer ability of catalysts. Nano-crystalline mesoporous

TS-1 (MTS-1) with mesopore size of ca. 3 nm and small crystal size (<100 nm) is successfully synthesized using the commercial soft template by dry-gel conversion method, and then used as support for Au deposition. Notably, it is found that Au/MTS-1 catalyst exhibits simultaneously enhanced PO selectivity (>95%) and high stability over 48 h, which are much better than traditional Au/TS-1 catalysts. The mechanism for the enhanced selectivity and stability is proposed by using multi-techniques such as HAADF-STEM, FT-IR, TGA-DTG and ^{29}Si MAS NMR. Compared with conventional Au/TS-1, the Au/MTS-1 catalyst has enhanced mass transfer ability by shortened reactant/product diffusion length and also better hydrophobicity, which result in reduced coke weight and absence of aromatic coke. The insights reported here may pave the way for the rational design of highly efficient zeolite supported metallic catalysts that suffers from poor selectivity and stability.

AUTHOR INFORMATION

Corresponding Author

Email for prof. Xinggui Zhou: xgzhou@ecust.edu.cn; Tel.: +86-21-64253509.

Email for prof. Chaohe Yang: yangch@upc.edu.cn; Tel.: +86-532-86984710.

Author Contributions

The manuscript was written through contributions of all authors. All authors have given approval to the final version of the manuscript.

ASSOCIATED CONTENT

Supporting Information. The structural properties of TS-1 and MTS-1 samples, HRTEM images of the Au/MTS-1 catalyst and ^{29}Si NMR spectra of MTS-1 and TS-1 samples. This material is available free of charge via the Internet at http://pubs.acs.org.

ACKNOWLEDGMENT

This work is supported by the Natural Science Foundation of China (21606254, 21476263); Natural Science Foundation of Shandong Province (ZR2016BB16); Joint Funds of petrochemical industry (U1462205); Special Grade of China Postdoctoral Science Foundation (2016T90657); China Postdoctoral Science Foundation (2015M582160).

REFERENCES

(1) Khatib, S. J.; Oyama, S. T. *Catal. Rev.* **2015**, 57, 306-344.

(2) Lee, W. S.; Cem Akatay, M.; Stach, E. A.; Ribeiro, F. H.; Delgass, W. N. *J. Catal.* **2012**, 287, 178-189.

(3) Haruta, M.; Uphade, B. S.; Tsubota, S.; Miyamoto, A. *Res. Chem. Intermed.* **1998**, 24, 329-336.

(4) Hayashi, T.; Tanaka, K.; Haruta, M. *J. Catal.* **1998**, 178, 566-575.

(5) Lee, W.S.; Lai, L.C; Cem Akatay, M.; Stach, E. A.; Ribeiro, F. H.; Delgass, N.W. *J. Catal.* **2012**, 296, 31-42.

(6) Chen, J.; Halin, S. J. A.; Pidko, E. A.; Verhoeven, M. W. G. M.; Ferrandez, D. M. P.; Hensen, E. J. M.; Schouten, J. C.; Nijhuis, T. A. *ChemCatChem* **2013**, 5, 467-478.

(7) Lu, X.; Zhao, G. F.; Lu, Y. *Catal. Sci. Technol.* **2013**, 3, 2906-2909.

(8) Sinha, A. K.; Seelan, S.; Tsubota, S.; Haruta, M. *Angew. Chem. Int. Ed.* **2004**, 43, 1546-1548.

(9) Feng, X.; Chen, D.; Zhou, X. *RSC Adv.* **2016**, 6, 44050-44056.

(10) Uphade, B. S.; Akita, T.; Nakamura, T.; Haruta, M. *J. Catal.* **2002**, 209, 331-340.

(11) Qi, C.; Huang, J.; Bao, S.; Su, H.; Akita, T.; Haruta, M. *J. Catal.* **2011**, 281, 12-20.

(12) Lu, J.; Zhang, X.; Bravo-Suárez, J. J.; Bando, K. K.; Fujitani, T.; Oyama, S. T. *J. Catal.* **2007**, 250, 350-359.

(13) Yang, H.; Tang, D.; Lu, X.; Yuan, Y. *J. Phys. Chem. C* **2009**, 113, 8186-8193.

(14) Feng, X.; Duan, X.; Qian, G.; Zhou, X.; Chen, D.; Yuan, W. *Appl. Catal. B* **2014**, 150, 396-401.

(15) Zhan, G.; Du, M.; Sun, D.; Huang, J.; Yang, X.; Ma, Y.; Ibrahim, A.-R.; Li, Q. *Ind. Eng. Chem. Res.* **2011**, 50, 9019-9026.

(16) Du, M.; Zhan, G.; Yang, X.; Wang, H.; Lin, W.; Zhou, Y.; Zhu, J.; Lin, L.; Huang, J.; Sun, D.; Jia, L.; Li, Q. *J. Catal.* **2011**, 283, 192-201.

(17) Huang, J.; Lima, E.; Akita, T.; Guzmán, A.; Qi, C.; Takei, T.; Haruta, M. *J. Catal.* **2011**, 278, 8-15.

(18) Huang, J.; Takei, T.; Akita, T.; Ohashi, H.; Haruta, M. *Appl. Catal. B* **2010**, 95, 430-438.

(19) Feng, X.; Liu, Y.; Li, Y.; Yang, C.; Zhang, Z.; Duan, X.; Zhou, X.; Chen, D. *AIChE J.* **2016**, 62, 3963-3972.

(20) Ruiz, A.; Van der Linden, B.; Makkee, M.; Mul, G. *J. Catal.* **2009**, 266, 286-290.

(21) Pérez-Ramírez, J.; Christensen, C. H.; Egeblad, K.; Christensen, C. H.; Groen, J. C. *Chem. Soc. Rev.* **2008**, 37, 2530-2542.

(22) Wang, H.; Pinnavaia, T. J. *Angew. Chem. Int. Ed.* **2006**, 45, 7603-7606.

(23) Yue, M. B.; Sun, M. N.; Xie, F.; Ren, D. D. *Microporous Mesoporous Mater.* **2014**, 183, 177-184.

(24) Taylor, B.; Lauterbach, J.; Delgass, W. N. *Catal. Today* **2007**, 123, 50-58.

(25) Schmidt, I.; Krogh, A.; Wienberg, K.; Carlsson, A.; Brorson, M.; Jacobsen, C. J. H. *Chem. Comm.* **2000**, 2157-2158.

(26) Khomane, R. B.; Kulkarni, B. D.; Paraskar, A.; Sainkar, S. R. *Mater. Chem. Phys.* **2002**, 76, 99-103.

(27) Takemura, K. *J. Appl. Phys.* **2001**, 89, 662-668.

(28) Wang, Z.; Xu, L.; Jiang, J.-g.; Liu, Y.; He, M.; Wu, P. *Microporous Mesoporous Mater.* **2012**, 156, 106-114.

(29) Mintova, S.; Hölzl, M.; Valtchev, V.; Mihailova, B.; Bouizi, Y.; Bein, T. *Chem. Mater.* **2004**, 16, 5452-5459.

(30) Xu, L.; Ren, Y.; Wu, H.; Liu, Y.; Wang, Z.; Zhang, Y.; Xu, J.; Peng, H.; Wu, P. *J. Mater. Chem.* **2011**, 21, 10852-10858.

(31) Serrano, D.; Sanz, R.; Pizarro, P.; Moreno, I.; Medina, S. *Appl. Catal. B* **2014**, 146, 35-42.

(32) Qi, C. *Gold Bull.* **2008**, 41, 224-234.

(33) Möller, K.; Yilmaz, B.; Jacubinas, R. M.; Müller, U.; Bein, T. *J. Am. Chem. Soc.* **2011**, 133, 5284-5295.

(34) Feng, X.; Duan, X.; Cheng, H.; Qian, G.; Chen, D.; Yuan, W.; Zhou, X. *J. Catal.* **2015**, 325, 128-135.

(35) Feng, X.; Duan, X.; Qian, G.; Zhou, X.; Chen, D.; Yuan, W. *J. Catal.* **2014**, 317, 99-104.

(36) Lee, W.S.; Cem Akatay, M.; Stach, E. A.; Ribeiro, F. H.; Delgass, W. N. *J. Catal.* **2013**, 308, 98-113.

(37) Feng, X.; Duan, X.Z.; Yang, J.; Qian, G.; Zhou, X.G.; Chen, D.; Yuan, W.K. *Chem. Eng. J.* **2015**, 278, 234-239.

(38) Edwards, J. K.; Solsona, B.; N, E. N.; Carley, A. F.; Herzing, A. A.; Kiely, C. J.; Hutchings, G. J. *Science* **2009**, 323, 1037-1041.

(39) Zhou, J.; Hua, Z.; Liu, Z.; Wu, W.; Zhu, Y.; Shi, J. *ACS Catal.* **2011**, 1, 287-291.

(40) Rollmann, L. D. *J. Catal.* **1977**, 47, 113-121.

(41) Wu, Z.; Goel, S.; Choi, M.; Iglesia, E. *J. Catal.* **2014**, 311, 458-468.

(42) Feng, X.; Chen, D.; Zhou, X. G. *RSC Adv.* **2016**, 6, 44050-44056.

(43) Du, S.; Chen, X.; Sun, Q.; Wang, N.; Jia, M.; Valtchev, V.; Yu, J. *Chem. Comm.* **2016**, 52, 3580-3583.

(44) Zhu, Y.; Hua, Z.; Zhou, X.; Song, Y.; Gong, Y.; Zhou, J.; Zhao, J.; Shi, J. *RSC Adv.* **2013**, 3, 4193-4198.

(45) Serrano, D.; Sanz, R.; Pizarro, P.; Moreno, I.; Shami, S. *Microporous and Mesoporous Mater.* **2014**, 189, 71-82.

(46) Jin, F.; Lin, T.-H.; Chang, C. C.; Wan, B. Z.; Lee, J. F.; Cheng, S. *RSC Adv.* **2015**, 5, 61710-61718.

(47) Chen, J.; Halin, S. J.; Pidko, E. A.; Verhoeven, M.; Ferrandez, D. M. P.; Hensen, E. J.; Schouten, J. C.; Nijhuis, T. A. *ChemCatChem* **2013**, 5, 467-478.

(48) Jin, F.; Wu, Y.; Liu, S.; Lin, T. H.; Lee, J. F.; Cheng, S. *Catal. Today* **2015**, 264, 98-108.

Table of Content